Supplementary Information

Ferroelectric 2D Antimony Oxides with Wide Bandgaps

Romakanta Bhattarai[a], Kai Ni[b], and Xiao Shen[a]*

[a]Department of Physics and Materials Science, The University of Memphis, Memphis, TN, USA

[b]Department of Electrical and Microelectronic Engineering, Rochester Institute of Technology, Rochester, NY, USA

*xshen1@memphis.edu

I. Computational Details

The computational study in this work is carried out as follows. First, we use the genetic algorithm in combination with the density functional theory (DFT) to search for stable structures corresponding to the local energy minimum. Initially, a set of 30 structures are generated randomly from the space group set, and this number is preserved in each generation afterward. The calculation is stopped when the most stable structure remains unchanged in the fifteen generations. The best candidates in every generation are used to produce the offspring for the next generation. Heredity accounts for half of the candidates in each generation. The remaining half is produced from the space group symmetry (20%), soft mutation (10%), lattice mutation (10%), and permutation (10%). During the search, the number of atoms are varied from 3 to 30 with the stoichiometry of Sb_2O_4. The searches are carried out for both 3D and 2D dimensions. We use the USPEX[1,2] code for the genetic algorithm and the VASP[3] code for DFT calculations, with the Perdew-Burke-Ernzerhof (PBE)[4] type of exchange and correlation functional and the projected augmented wave (PAW)[5] type pseudopotential. The electronic and ionic convergence conditions are set to 10^{-5} and 10^{-4} eV, respectively, along with the plane-wave basis set having a maximum energy cutoff of 320 eV. The electric dipole moments in γ-Sb_2O_4 and δ-Sb_2O_4 phases are calculated using the Berry-phase method.[6,7]

The most stable structures predicted from the USPEX are relaxed in a tighter convergence criterion. A plane-wave basis set with the energy cutoff of 500 eV, in addition to the thresholds of 10^{-9} eV and 10^{-4} eV/Å for the electronic energy and force convergence, are considered in these calculations. For the integration of the Brillouin zone, Γ-centered k-points grids of 15 × 15 × 15 and 15 × 15 × 1 are chosen for the bulk and the corresponding monolayers, respectively. The dynamical stability of the predicted structures

is tested using their respective supercells implemented in the Phonopy package,[8] which works under the finite displacement method. Furthermore, the thermal stability is confirmed by performing the ab initio molecular dynamics simulations at 500 K for 30 ps.

The energy barrier for switching is calculated using the solid-state nudged elastic band (SS-NEB) method.[9] The convergence criterion is set such that the force between any two successive steps is less than 0.01 eV/Å. The Raman spectra of the predicted structures are calculated using the density functional perturbation theory as implemented in the Quantum Espresso package.[10] Norm-conserving pseudopotentials generated via Rappe-Rabe-Kaxiras-Joannopoulos (RRKJ)[11] scheme along with the PBE functional is used. The energy cutoff for the plane-wave basis set is 80 Rydberg. The total energy convergence criteria are set to 10^{-12}, and 10^{-14} Ry, respectively, for the self-consistency and the phonon calculations.

II. Stability of γ- and δ-Sb_2O_4 Monolayers

We construct the monolayers of γ- and δ-Sb_2O_4 and test the dynamical stabilities. First, we calculate the interlayer coupling energies and plot them as functions of interlayer distances, as shown in Fig. S1. The plots confirm that the monolayers are energetically stable and indicate the possibility of experimental synthesis of these monolayers.

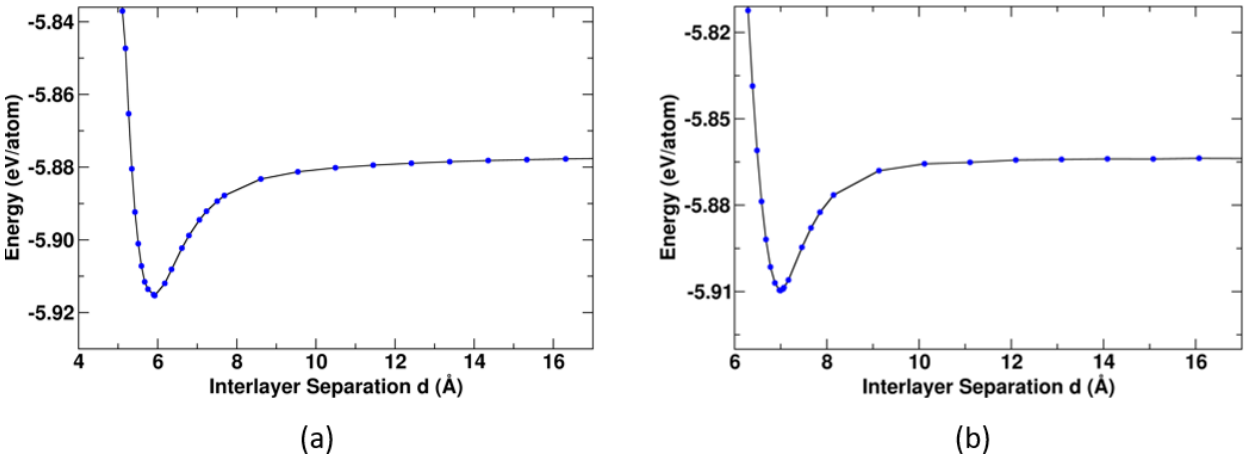

Figure S1: Coupling energy of as a function of interlayer separation (a) γ-Sb_2O_4, and (b) δ-Sb_2O_4

We then test the dynamical stability of all phases by calculating the phonon spectra using the Phonopy[8] package. Since we have confirmed that the monolayer of γ- and δ-Sb_2O_4 are energetically stable, testing the dynamical stability of these monolayers should be sufficient for the dynamical stability of the corresponding bulk phases. Therefore, we present the phonon dispersion spectra of γ- and δ-Sb_2O_4 monolayers in Figs. S2(a), and S3(a), respectively. There are no sizable imaginary frequencies in the phonon spectra in any case, which indicates that the corresponding structures are dynamically stable. A very small imaginary

frequency appears near the Γ point in the γ-Sb_2O_4 phase, which is because of the numerical artifacts in the calculations. This could be removed by using larger supercell sizes or increasing the precisions (increased sampling points, larger energy cutoff, and tightening the criteria for electronic convergence).

In addition, we also test the thermal stability of the monolayers by performing the ab initio molecular dynamics (AIMD) simulation at an elevated temperature. The AIMD simulations are carried out in supercells of monolayers at 500 K for 30 ps with a time step of 2 fs. The potential energy profiles are plotted as a function of time, as shown in Figs. S2(b) and S3(b), for γ- and δ-Sb_2O_4 monolayers, respectively. Inserts represent the corresponding snapshots of the structures during the simulation. No sudden drop of the fluctuating potential energy, as well as no structure reconstruction throughout the simulation time, is observed, which implies the thermal stability of the structures.

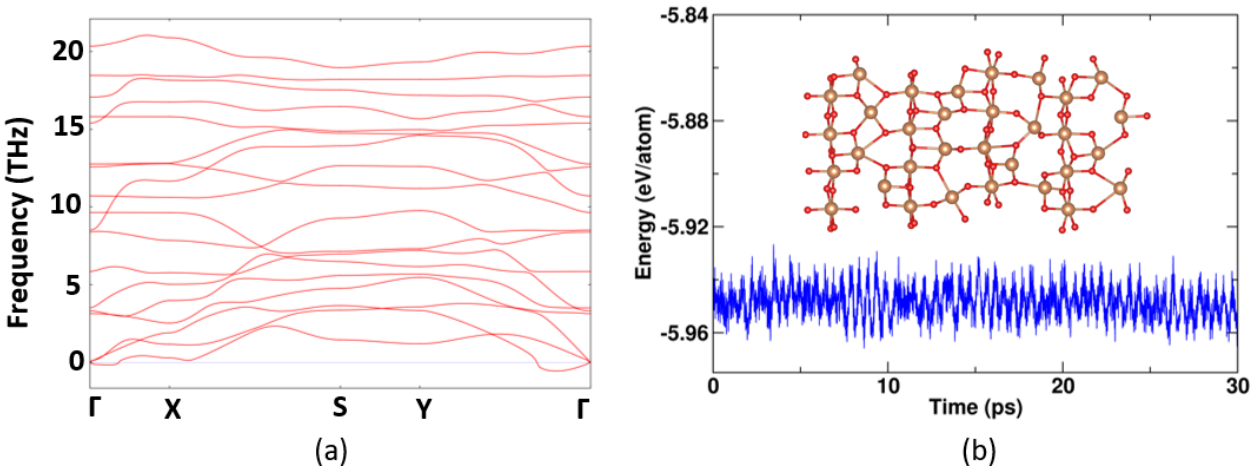

Figure S2: (a) Phonon band structures of monolayer γ-Sb_2O_4 (b) Potential energy profile of AIMD simulation of monolayer γ-Sb_2O_4 at 500 K for 30 ps. Insert shows a snapshot of structure during the simulation.

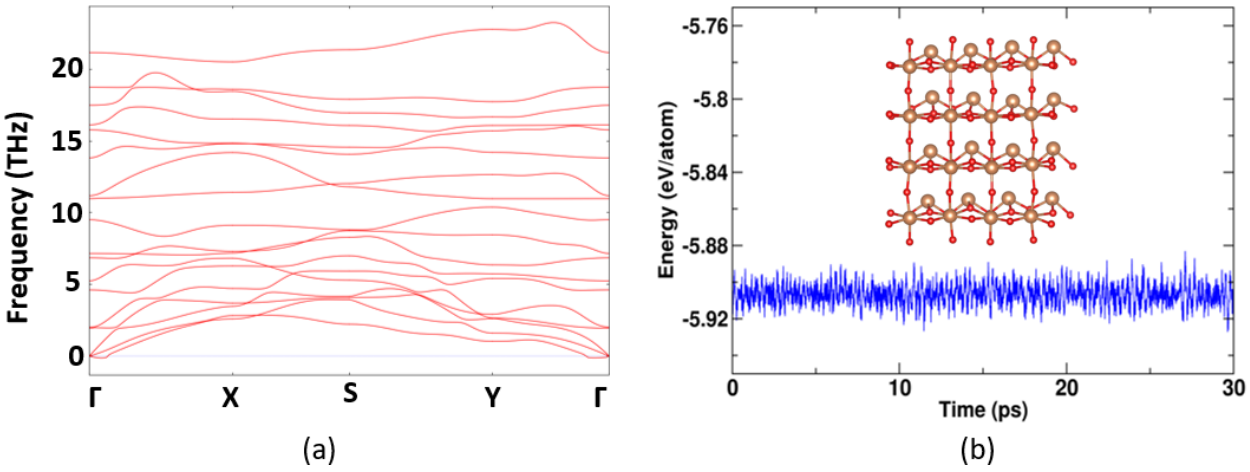

Figure S3: (a) Phonon band structures of monolayer δ-Sb_2O_4 (b) Potential energy profile of AIMD simulation of monolayer δ-Sb_2O_4 at 500 K for 30 ps. Insert shows a snapshot of structure during the simulation.

In addition to thermodynamic stability, we also examine the chemical stability of γ- and δ-Sb_2O_4 by investigating the adsorption of CO_2 and H_2O following the method described in Ref. 12. The calculated adsorption energies of CO_2 on γ- and δ-Sb_2O_4 are 0.13 and 0.03 eV/molecule, respectively. The adsorption energies of H_2O on γ- and δ-Sb_2O_4 are 0.49 and 0.54 eV/molecule, respectively. The adsorption geometries are shown in Fig. S4. These results indicate that CO_2 interacts with the surface of 2D Sb_2O_4 by van der Waals force, while H_2O interacts through hydrogen bonding. No chemisorption is observed in either case, indicating the chemical stability of γ- and δ-Sb_2O_4 against CO_2 and H_2O in the ambient environment.

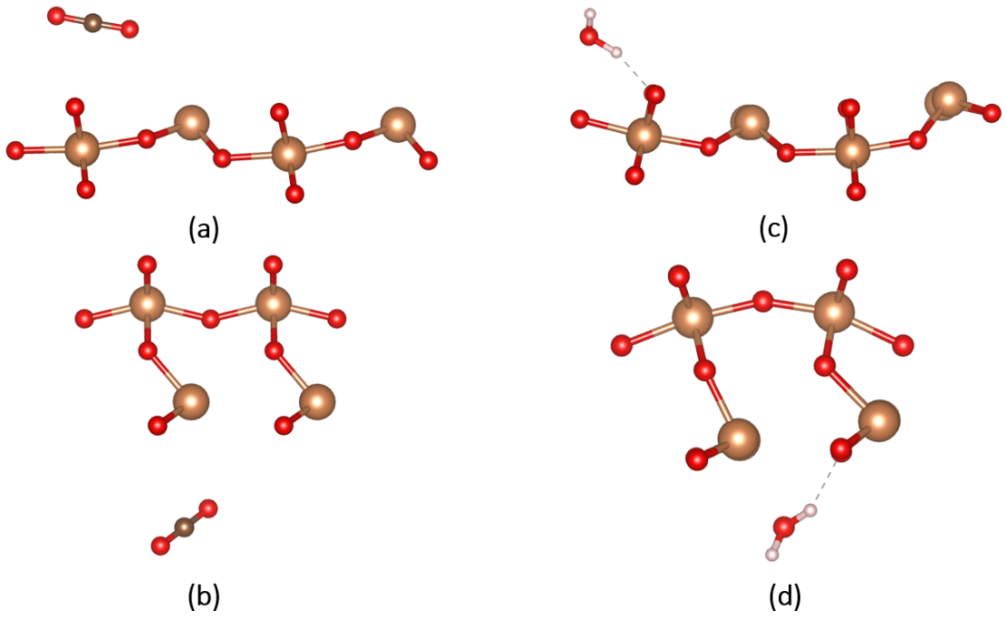

Figure S4: Adsorption geometry of a CO_2 molecule on γ-Sb_2O_4 (a) and δ-Sb_2O_4 (b). Adsorption geometry of a H_2O molecule on γ-Sb_2O_4 (c) and δ-Sb_2O_4 (d).

III. Bonding Analysis on γ- and δ-Sb_2O_4

To get a deeper insight into the bonding nature among γ- and δ-Sb_2O_4, we plot each phase separately, highlighting every Sb-O bond in Fig. S5. Each ion is labeled to facilitate comparison with the bond lengths in Table S1.

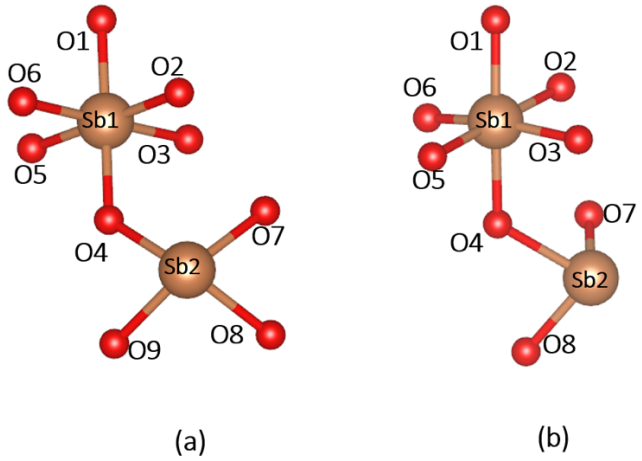

Figure S5: Bonding environments of Sb ions in (a) γ-Sb_2O_4, and (b) δ-Sb_2O_4

The structural configuration of γ-Sb_2O_4 looks similar to δ-Sb_2O_4; however, in reality, they differ in various aspects, including bond lengths, bond angles, et al., which give rise to separate properties between them. Table S1 below compares the bonding environments between the two Sb_2O_4 structures.

Table S1: Comparison of bonding environments among γ-Sb_2O_4, and δ-Sb_2O_4

Phases	Bonding pairs	Bond lengths (Å)	Bonding pairs	Bond lengths (Å)
γ-Sb_2O_4 (bulk)	Sb1-O1	2.067	Sb2-O4	2.153
	Sb1-O2	2.012	Sb2-O7	2.159
	Sb1-O3	2.028	Sb2-O8	2.148
	Sb1-O4	2.054	Sb2-O9	2.157
	Sb1-O5	2.027		
	Sb1-O6	2.012		
γ-Sb_2O_4 (monolayer)	Sb1-O1	2.116	Sb2-O4	2.159
	Sb1-O2	2.038	Sb2-O7	2.159
	Sb1-O3	1.991	Sb2-O8	2.128

	Sb1-O4 Sb1-O5 Sb1-O6	2.055 1.991 2.038	Sb2-O9	2.128
δ-Sb_2O_4 (bulk)	Sb1-O1 Sb1-O2 Sb1-O3 Sb1-O4 Sb1-O5 Sb1-O6	2.051 2.080 1.966 2.080 1.051 1.957	Sb2-O4 Sb2-O7 Sb2-O8	2.213 2.019 2.019
δ-Sb_2O_4 (monolayer)	Sb1-O1 Sb1-O2 Sb1-O3 Sb1-O4 Sb1-O5 Sb1-O6	1.992 2.137 2.001 2.138 1.992 1.993	Sb2-O4 Sb2-O7 Sb2-O8	2.070 2.025 2.025

IV. Vibrational Modes

Both γ-Sb_2O_4 and δ-Sb_2O_4 have eighteen vibrational modes, as each unit cell contains six atoms in both phases. We tabulate the frequencies of these modes in Table S2, followed by plotting the vibrational eigenvectors in their bulk phases. We believe the results can be helpful for searching for these phases experimentally.

Table S2: Raman modes and corresponding vibrational frequencies of γ-Sb_2O_4, and δ-Sb_2O_4

Mode	γ-Sb_2O_4 bulk (cm^{-1})	γ-Sb_2O_4 monolayer (cm^{-1})	δ-Sb_2O_4 bulk (cm^{-1})	δ-Sb_2O_4 monolayer (cm^{-1})
1	0	0	0	0
2	0	0	0	0
3	0	0	0	0
4	42	107	87	63
5	86	122	96	67
6	136	141	128	155
7	214	191	137	162
8	284	284	216	232

9	311	301	273	240
10	328	321	281	327
11	354	346	349	370
12	388	427	442	378
13	424	444	454	445
14	505	525	475	526
15	525	525	495	542
16	539	558	511	591
17	583	610	635	629
18	682	699	794	758

The first three modes in each phase having zero vibrational frequency represent the collective translational motion of the crystal units in the same direction (see below). The corresponding vibrational modes are presented in Figures S6 and S7. The antimony and oxygen atoms are represented by gray and red colors, respectively. The directions of displacements are shown by green arrows.

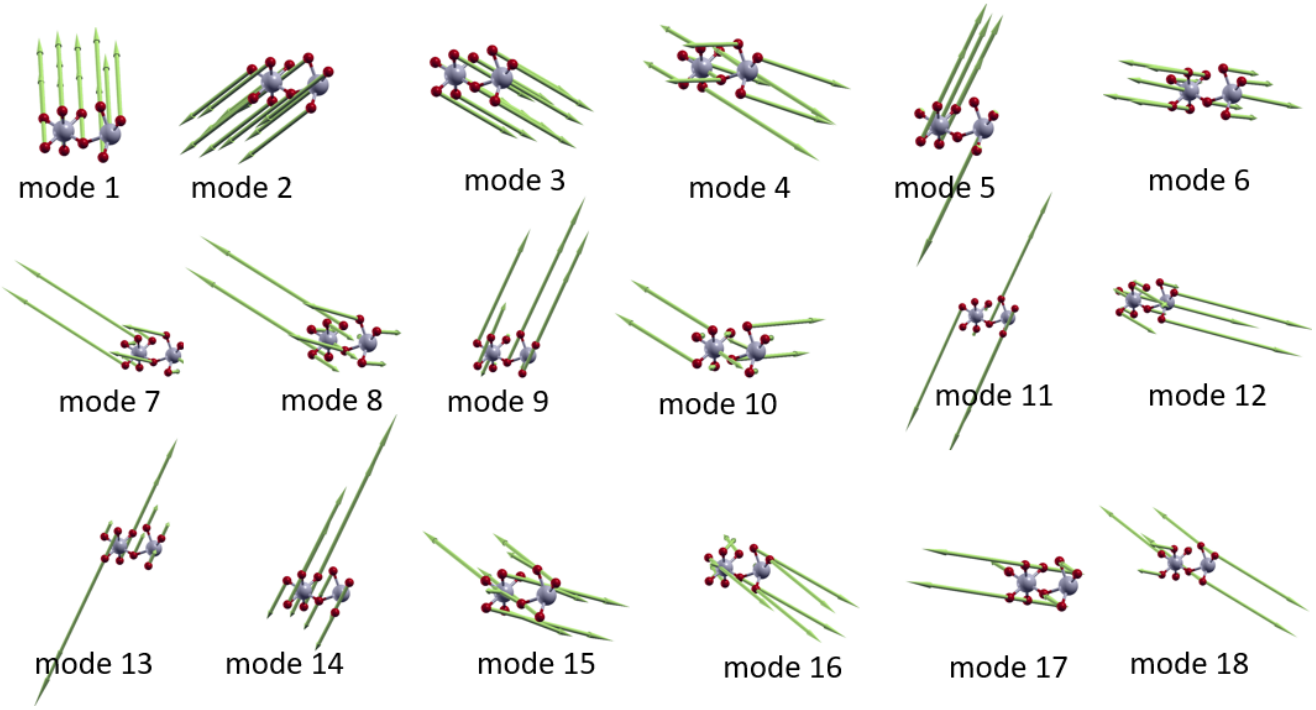

Figure S6: Eighteen vibrational modes of bulk γ-Sb_2O_4.

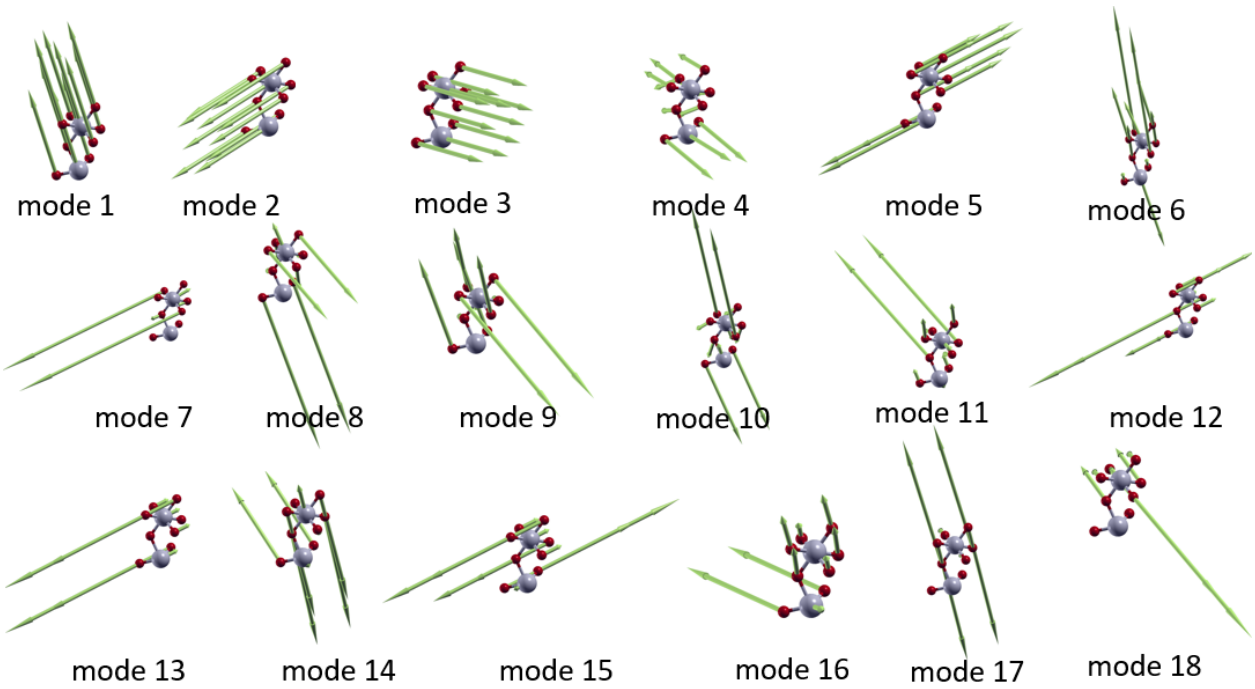

Figure S7: Eighteen vibrational modes of bulk δ-Sb_2O_4.

V. X-Ray Diffraction (XRD) Spectra

In addition to Raman spectra, we also present the simulated XRD results using Cu-k alpha method in Table S3 below to further help the experimental investigations.

Table S3: Simulated XRD results of bulk γ-Sb_2O_4, and δ-Sb_2O_4 using Cu-k alpha method

S. N.	γ-Sb_2O_4 2θ (°)	δ-Sb_2O_4 2θ (°)
1	15.852	23.499
2	16.571	24.179
3	18.160	26.136
4	27.040	29.456
5	30.019	30.951
6	31.202	36.848
7	32.171	37.303
8	33.501	38.655

9	36.839	39.351
10	37.499	41.070
11	40.404	46.826
12	47.924	49.224
13	48.491	50.768
14	49.261	53.763
15	50.087	55.432
16	51.112	56.536
17	53.938	57.813
18	55.800	59.478
19	60.314	63.516
20	62.029	64.505
21	67.293	68.524

The XRD data are then plotted by showing the corresponding miller indices (hkl) in Figure S8 below.

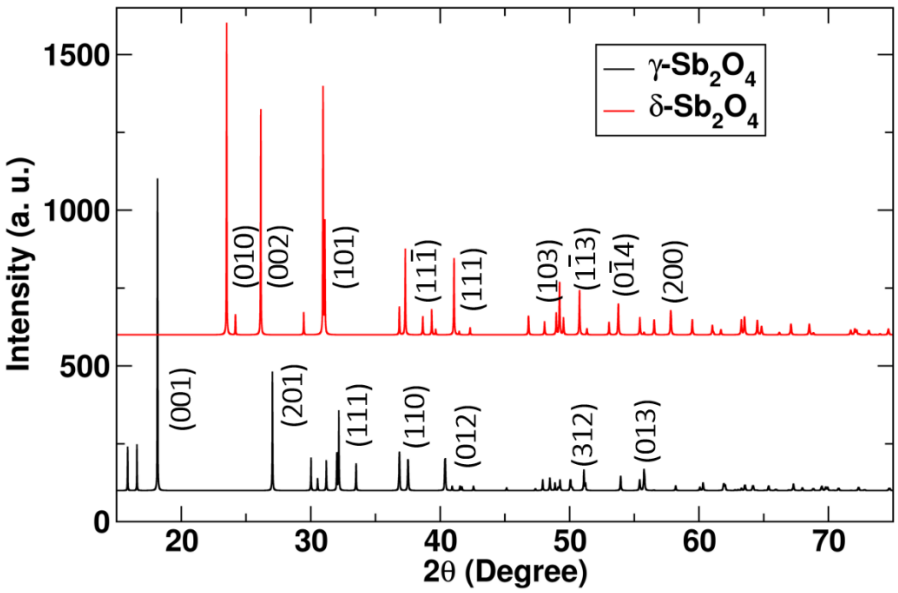

Figure S8: Plot of simulated XRD spectra of bulk γ-Sb_2O_4, and δ-Sb_2O_4 using Cu-k alpha method

VI. Densities of States of Doped Sb_2O_4

We calculated the bandgaps of Bi-doped γ-Sb_2O_4 and As-doped δ-Sb_2O_4 using the DFT method. The calculated bandgaps of Bi-doped γ-Sb_2O_4 and As-doped δ-Sb_2O_4 are 1.99 and 1.41 eV, respectively. The densities of states (DOS) in both cases are shown in Fig. S9.

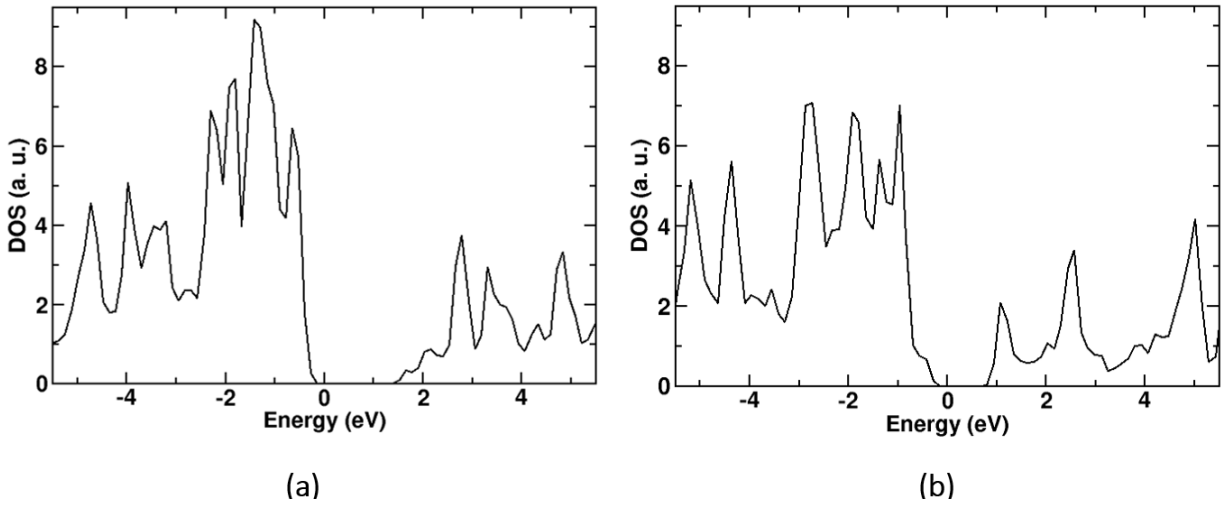

Figure S9: DOS plots of (a) Bi-doped γ-Sb_2O_4, and (b) As-doped δ-Sb_2O_4.

References:

1. Oganov, A. R., Lyakhov, A. O. & Valle, M. How Evolutionary Crystal Structure Prediction Works—and Why. *Acc. Chem. Res.* **44**, 227–237 (2011).
2. Lyakhov, A. O., Oganov, A. R., Stokes, H. T. & Zhu, Q. New developments in evolutionary structure prediction algorithm USPEX. *Comput. Phys. Commun.* **184**, 1172–1182 (2013).
3. Kresse, G. & Furthmüller, J. Efficient iterative schemes for ab initio total-energy calculations using a plane-wave basis set. *Phys. Rev. B* **54**, 11169–11186 (1996).
4. Perdew, J. P., Burke, K. & Ernzerhof, M. Generalized Gradient Approximation Made Simple. *Phys. Rev. Lett.* **77**, 3865–3868 (1996).
5. Blöchl, P. E. Projector augmented-wave method. *Phys. Rev. B* **50**, 17953–17979 (1994).
6. King-Smith, R. D. & Vanderbilt, D. Theory of polarization of crystalline solids. *Phys. Rev. B* **47**, 1651–1654 (1993).

7. Vanderbilt, D. & King-Smith, R. D. Electric polarization as a bulk quantity and its relation to surface charge. *Phys. Rev. B* **48**, 4442–4455 (1993).
8. Togo, A. & Tanaka, I. First principles phonon calculations in materials science. *Scr. Mater.* **108**, 1–5 (2015).
9. Sheppard, D., Xiao, P., Chemelewski, W., Johnson, D. D. & Henkelman, G. A generalized solid-state nudged elastic band method. *J. Chem. Phys.* **136**, 074103 (2012).
10. Giannozzi, P. *et al.* QUANTUM ESPRESSO: a modular and open-source software project for quantum simulations of materials. *J. Phys. Condens. Matter* **21**, 395502 (2009).
11. Rappe, A. M., Rabe, K. M., Kaxiras, E. & Joannopoulos, J. D. Optimized pseudopotentials. *Phys. Rev. B* **41**, 1227–1230 (1990).
12. Tang, X., Shang, J., Gu, Y., Du, A. & Kou, L. Reversible gas capture using a ferroelectric switch and 2D molecule multiferroics on the In2Se3 monolayer. *J. Mater. Chem. A* **8**, 7331–7338 (2020).